Ionospheric response during low and high solar activity

Vaishnav, R.[1*], Jacobi, Ch.[1], Berdermann, J.[2], Schmölter, E.[2], Codrescu, M.[3]

[1]*Leipzig Institute for Meteorology, Universität Leipzig, Stephanstr. 3, 04103 Leipzig, Germany (rajesh_ishwardas.vaishnav@uni-leipzig.de)*
[2]*German Aerospace Center, Kalkhorstweg 53, 17235 Neustrelitz, Germany*
[3]*Space Weather Prediction Centre, National Oceanic and Atmospheric Administration, Boulder, Colorado, USA.*

Summary: We analyse solar extreme ultraviolet (EUV) irradiance observed by the Solar EUV Experiment (SEE) onboard the Thermosphere Ionosphere Mesosphere Energetics and Dynamics (TIMED) satellite, and solar proxies (the F10.7 index, and Mg-II index), and compare their variability with the one of the global mean Total Electron Content (GTEC). Cross-wavelet analysis confirms the joint 27 days periodicity in GTEC and solar proxies. We focus on a comparison for solar minimum (2007-2009) and maximum (2013-2015) and find significant differences in the correlation during low and high solar activity years. GTEC is delayed by approximately 1-2 days in comparison to solar proxies during both low and high solar activity at the 27 days solar rotation period. To investigate the dynamics of the delay process, Coupled Thermosphere Ionosphere Plasmasphere electrodynamics model simulations have been performed for low and high solar activity conditions. Preliminary results using cross correlation analysis show an ionospheric delay of 1 day in GTEC with respect to the F10.7 index during low and high solar activity.

Zusammenfassung: Wir analysieren vom Solar Extreme Ultraviolet Experiment (SEE) an Bord des Thermosphere-Ionosphere-Mesosphere Energetics and Dynamics (TIMED) Satelliten gemessene solare EUV-Irradianzen, solare Proxies (den F10.7-Index und denMg-II-Index), und vergleichen deren Variabilität mit derjenigen des global gemittelten Gesamtelektronengehalts (GTEC). Kreuzwaveletanalysen bestätigen eine gemeinsame Variabilität im Periodenbereich der solaren Rotation (27 Tage). Wir vergleichen insbesondere den Zusammenhang während des solaren Minimums (2007-2009) und Maximums (2013-2015), wobei signifikante Unterschiede der Korrelation zwischen solaren und ionosphärischen Parametern auftreten. Es tritt eine Verzögerung der Maxima und Minima von GTEC gegenüber denjenigen der solaren Proxies von einem Tag sowohl im solaren Minimum als auch im solaren Maximum auf.

1. Introduction

The existence of the ionized layer in the atmosphere is due to the incoming solar radiation ranging from X-rays to the extreme ultraviolet (EUV, 0-105 nm). Solar input significantly changes the behavior of the thermosphere/ionosphere system during low and high solar activity, modulated at different time scales including the 11 years solar cycle and the 27 days solar rotation period, as has been shown using various solar proxies (e.g., Jakowski et al., 1991; Liu et al., 2003; Afraimovich et al., 2008; Liu and Chen 2009; Astafyeva et al., 2008; Chen et al., 2015; Patel et al., 2017). Solar EUV

modulations are stronger during high solar activity as compared to low solar activity. The ionosphere region (80-500 km) may be characterized by the total electron content (TEC, given in TEC units (TECU), 1 TECU = 10^{16} electrons/m^2) (e.g., Kane, 1992; Liu et al., 2006). TEC is one of the most important ionospheric parameters, which is frequently used to represent the behavior of the ionosphere. It varies temporally and spatially due to the complex interaction with the solar radiations (e.g., Mukhtarov et al., 2013).

Many researchers have explored possible relations between the solar radiation and the ionosphere (e.g. Jakowski et al., 1991; Afraimovich et al., 2008; Min et al., 2009; Lee et al., 2012; Jacobi et al., 2016). To establish possible relations of solar input and TEC, solar proxies are used as a representative of solar EUV with ionospheric TEC. Solar proxies are not always capable to sufficiently reproduce the EUV variability (Dudok de Wit et al., 2009), but they are often used due to unavailability of the direct EUV measurements. Most commonly used solar proxies are the solar radio flux at 10.7 cm (F10.7 index, given in solar flux units (sfu), 1 sfu = 10^{-22}Wm^{-2} Hz^{-1}) (Tapping, 2013), the Mg-II index (core to wing ratio of MG-II line at 280 nm) (Maruyama, 2010), or the sunspot number (number of active formations) (Wolf, 1856). Direct continuous measurements of EUV from space are available since 2002 from the Solar EUV Experiment (SEE) onboard the Thermosphere-Ionosphere-Mesosphere Energetics and Dynamics (TIMED) satellite (Woods et al., 2000, 2005). However, due to degradation of EUV measuring instruments, solar proxies may be more suitable (BenMoussa et al., 2013), or repeated calibration is necessary.

Several authors have reported an approximately 1-day delay in TEC in comparison to solar indices (Jakowski et al., 1991; Su et al., 1999; Forbes et al., 2000; Liu et al., 2006; Afraimovich et al., 2008; Lee et al., 2012; Jacobi et al., 2016; see also references therein). The dynamics behind the delay observed in the ionospheric TEC with respect to the solar proxies is still an open question. Jakowski et al. (1991) suggested that it might be due to slow diffusion of atomic oxygen, which has a longer lifetime at 180 km altitude, and which is produced via photodissociation of molecular oxygen in the lower thermosphere.

The availability of general circulation models (GCM) gives us the opportunity to explore different atmospheric processes which may play an important role in the modulation of the ionosphere. Some frequently used GCMs are the Thermosphere Ionosphere Electrodynamics General Circulation Model (TIEGCM, Richmond et al., 1992), the Coupled Thermosphere Ionosphere Plasmasphere Electrodynamics (CTIPe, Fuller-Rowell and Rees, 1983**;** Codrescu et al., 2012), and the Global Ionosphere Thermosphere Model (GITM, Ridley et al., 2006). Most of the upper atmospheric models use the F10.7 index, the Mg-II index, or a modified F10.7 index to prescribe the solar variability and initialize the EUV parameterization routine.

It is essential to understand the fundamental behavior of the ionosphere during both low and high solar activity. Therefore, this study is focused on finding the correlation and time delay between global mean TEC (GTEC) and solar proxies during a low solar activity (January 2007 - December 2009) and a high solar activity (January 2013 - December 2015) period. To derive the periodicities in the GTEC and solar parameters, the cross-wavelet method will be utilized. Preliminary results of the CTIPe model to estimate the delay during low and high solar activity will also be presented.

2. Data and model description

2.1. Data sources

We have computed daily GTEC values using global ionospheric maps available from the International GNSS Service (IGS, Hernandez-Pajares et al., 2009) provided by NASA's data archive service (CDDIS, 2017). IGS-TEC maps are available in a latitude/longitude resolution of 2.5°/ 5° with a time resolution of 2 hours. To represent the solar variability, numerous solar proxies are available. We use daily values of F10.7 and the Bremen composite Mg-II index (Snow et al., 2014). The F10.7 index and the TIMED/SEE integrated EUV flux datasets are taken from the LISIRD (DeWolfe et al., 2010) database. Direct EUV measurements are available from the TIMED satellite. The NASA TIMED satellite was launched in 2001 and carries four instruments (GUVI, SABER, SEE and TIDI), orbiting at an altitude of 625 km (Woods et al., 2005). TIMED measures atmospheric density, temperatures, winds, and solar ultraviolet radiation. TIMED/SEE provides solar EUV irradiance measurements since January 22, 2002. The instrument is designed to measure the soft X-rays and EUV/UV radiation from 0.1 to 193 nm with a spectral resolution of 0.1nm. SEE includes two instruments, the EUV grating spectrograph and the XUV (soft x-rays) photometer system (Woods et al., 2000). We have used the daily integrated value of solar irradiance from 5.5 to 105.5 nm.

2.2. CTIPe model description

The CTIPe model is a global, 3-D, time-dependent, nonlinear, physics-based numerical model. It consists of four components, namely (a) a neutral thermosphere model (Fuller-Rowell and Rees, 1980), (b) a mid- and high-latitude ionosphere convection model (Quegan et al., 1982), (c) a plasmasphere and low latitude ionosphere (Millward et al., 1996), and (d) a self-consistent electrodynamics model (Richmond et al., 1992), which run simultaneously and are fully coupled. The thermosphere model solves the equations of momentum, continuity, and energy to calculate global temperature, density, wind components, and atmospheric neutral composition. The numerical solution of the composition equation with the energy and momentum equations describe the transport, turbulence, and diffusion of atomic oxygen, molecular oxygen and nitrogen (Fuller-Rowell and Rees, 1983). The latitude/longitude resolution is 2°/18°.

In the vertical direction, the atmosphere is divided into 15 levels in logarithmic pressure from 1 Pa to $8.73 \cdot 10^{-7}$ Pa with a step of one scale height. The corresponding geometric heights are variable depending on temperature. External inputs like solar UV and EUV, Weimer electric field, TIROS/NOAA auroral precipitation, and tidal forcing are required to drive the model. The F10.7 index is used as input proxy to drive the ionization, photodissociation and heating rates. The lower boundary is characterised by output of the Whole Atmospheric model (WAM, Akmaev, 2011). The F10.7 index is used in an artificial manner as input solar proxy to calculate ionization, heating, and oxygen dissociation processes in the ionosphere. For the simulation, a reference solar spectrum based on the EUV flux model for Aeronomic Calculations (EUVAC) (Richards et al., 1994), driven by variations of input F10.7 is used in the model. More description of CTIPe is available in Codrescu et al. (2008, 2012).

3. Results and discussion

3.1. Variation in TEC and solar EUV proxies

Here we have filtered the datasets using a low pass filter with a cut off period of three months. The filtered datasets have been normalized by subtracting the average value of the respective study period and dividing by the standard deviation. Figure 1 shows the normalized time series of GTEC, daily integrated SEE-EUV flux, F10.7 index, and MG-II index, while the curves are offset by 2 each. Figure 1(a) shows the data during the extended part of solar cycle 23 from 2007 to 2009. During this period solar activity was extremely low, which is also the case for the 27-day amplitudes. In comparison to the low solar activity years, Figure 1(b) shows stronger activity at the 27 days solar rotation period for the years of higher solar activity (2013-2015).

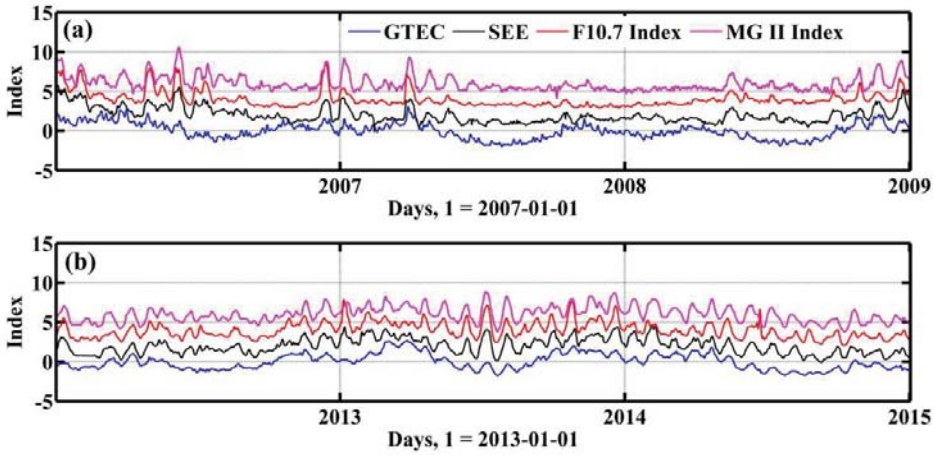

Fig. 1. Temporal variations of normalized datasets of GTEC (blue), SEE-EUV flux (black), F10.7 index (red), and Mg-II index (magenta) during (a) low (2007-2009) and (b) high (2013-2015) solar activity years. The curves are vertically offset by 2 each.

As shown in Figure 2(a), weaker correlation is observed during the low solar activity years between TEC and both the solar proxies in comparison to high solar activity years. During low solar activity years, the F10.7 index shows weaker correlation with the GTEC (Chen et al., 2011). In the correlation analysis during low (high) solar activity cycle, a correlation coefficient of 0.59 (0.77), 0.48 (0.64), and 0.50 (0.70) has been observed between normalized TEC and integrated EUV flux (black), F10.7 index (red), and MG-II index (figure not shown) respectively. The possible reason for the weaker correlation during low solar activity is the tidal forcing from the lower atmosphere, resulting in variability of GTEC (Lee et al., 2012). A strong correlation has been observed during high solar activity years. Mg-II index and SEE EUV flux shows stronger correlation with TEC than the F10.7 index. Jacobi et al. (2016) analyzed GTEC and Solar Dynamic Observatory/Extreme Ultraviolet Variability Experiment (SDO/EVE) integrated EUV flux data from 2011 to 2014 and they found a correlation of about 0.89. In comparison to the F10.7 index and sunspot number, solar EUV flux shows stronger correlation with GPS-TEC during the years 2010 to 2014

(Patel et al., 2017). Furthermore, to estimate the delay in GTEC with respect to solar proxies, the cross-correlation method has been used. In comparison to GTEC, all the solar proxies show a delay of 1-2 days. This means that solar radiation variations take about 1-2 days to influence the ionosphere. Various authors reported a similar ionospheric delay using solar proxies and GTEC (Jakoswki et al., 1991; Lee et al., 2012; Jacobi et al., 2016). According to Jakowski et al. (1991) this is possibly due to slow diffusion of atomic oxygen at 180 km or vertical transport processes.

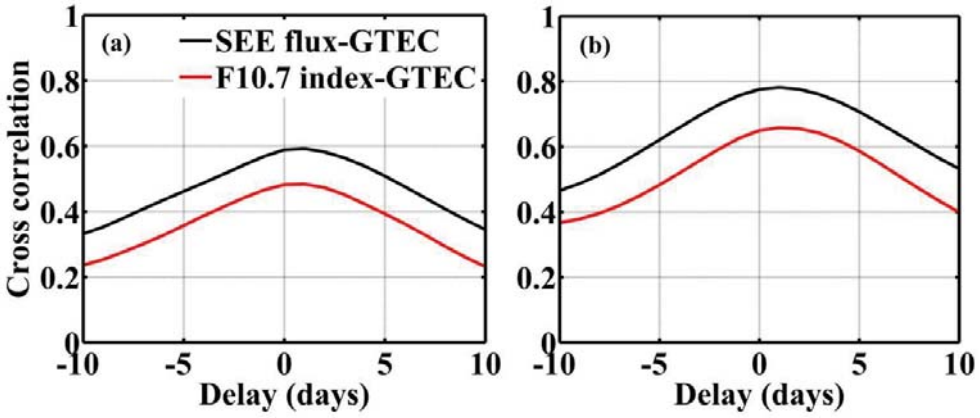

Fig. 2. Cross-correlation of GTEC with the SEE-EUV flux (black) and the F10.7 index (red) during (a) low (2007- 2009) and (b) high (2013-2015) solar activity years. Positive values denote GTEC lagging SEE-EUV or F10.7.

3.2. Wavelet analysis

To further investigate the nature of the relation between oscillations in the solar proxies and GTEC, the cross-wavelet technique has been used (Grinsted et al., 2004). This method indicates common high energy and relative phase between two-time series. Two continuous wavelet transforms using Morlet wavelet as mother function have been constructed.

Figure 3(a-b) shows the cross-wavelet spectra between GTEC with SEE–EUV flux (upper panel) and F10.7 (lower panel) index are during low solar activity years (left) and 3(c-d) during high solar activity years (right). All datasets have been normalized as described in section 3.1. From the figure, it is visible that during low solar activity the cross-wavelet spectra show weak power at the 27 days periodicity. In contrast to low solar activity years, a high energy region is observed at the 27 days periodicity during 2013-2015. All the arrows in the significant region show that GTEC is in phase with SEE and F10.7 index at 27 days periodicity. Thus, from this Figure it can be concluded that solar proxies influence GTEC mainly at the 27 days solar rotation period, which indicates that the solar forcing is strongly affecting the ionospheric activity. Guo et al. (2015) used the cross-wavelet and wavelet coherence methods to estimate the relation between TEC and sunspot numbers during the years 1999 to 2013. They found strong coherence at the solar rotation period, except for the extended solar minima years 2008-2009.

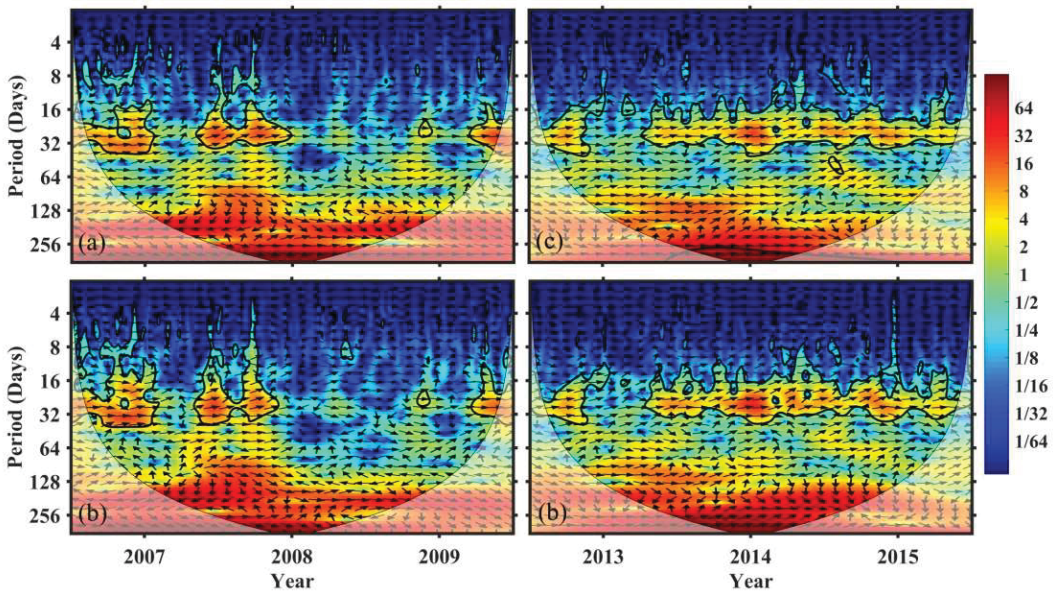

Fig. 3. Upper row: cross-wavelet transform of GTEC with (upper row) SEE-EUV flux and (lower row) F10.7 index during (a-b) low (2007- 2009) and (c-d) high (2013-2015) solar activity years. The cone of influence is shown by a black line. The arrow shows the phase relationship: in-phase pointing right, anti-phase pointing left and down-ward direction means that TEC is leading.

3.3. CTIPe simulated 27 days variation in TEC

The CTIPe model has been used to understand the role of solar EUV radiation in the ionospheric TEC variations. The F10.7 index is used as a model input. During the experiments, the model was run for 30 days by keeping all input parameters constant to attain the diurnally reproducible state and after this spin-up, the input was modified. We have used constant atmospheric conditions for 15 March 2013, and run the model by varying the F10.7 index for the 27 days solar rotation period.

The behavior of the ionosphere varies with solar activity. To understand this concept, we ran the CTIPe model for both low and high solar activity conditions. The F10.7 index was selected for low (70-75 sfu) and high (100-140 sfu) solar activity as shown in Figure 4(a, b), respectively, as a line plot. The simulated zonal mean TEC is shown in Figure 4 as background contour plot. The figure shows the variation in the output TEC with respect to the solar activity. Solar activity controls the ionization process in the ionosphere, which results in increase or decrease of the electron density. The model is capable to simulate the TEC distribution according to input solar activity. The electron density enhancement at low latitudes is due to the fountain effect (Appleton 1946).

As with the data analysis in section 3.1, we utilize the cross-correlation method to estimate the time delay between CTIPe simulated GTEC data and input F10.7 index for low and high solar activity, as shown in Figure 4(c,d). An ionospheric delay of about 1 day in GTEC with respect to the F10.7 index during low and high solar activity years

is observed. Note that in comparison to low solar activity, weaker correlation is observed during high solar activity conditions, which is not supported by the observations. A possible reason is that during solar maximum, EUV varies at different time scales, leading to considerable variability not necessarily directly correlated with TEC, which is not reproduced in our model experiment, where the F10.7 variability was chosen as purely sinusoidal.

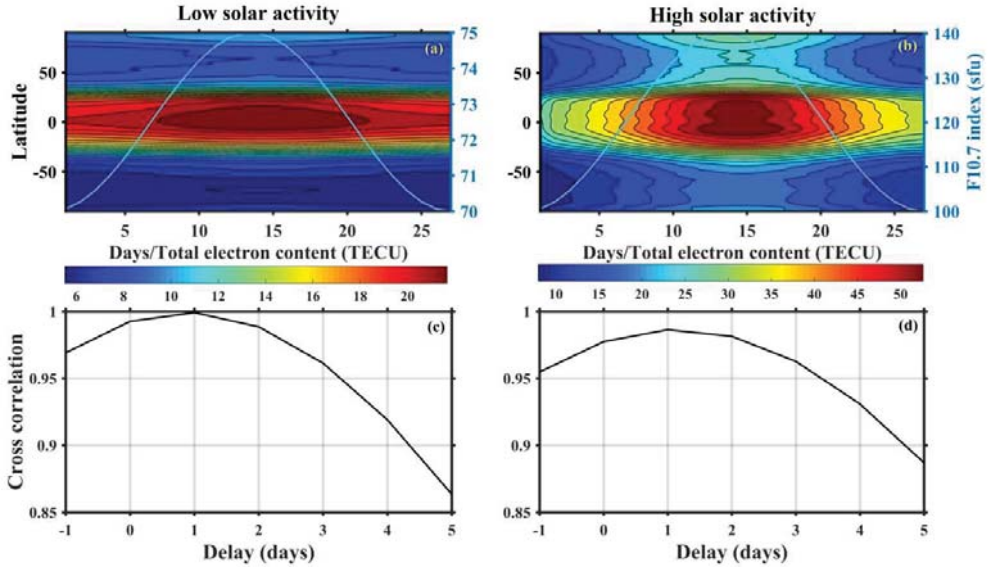

Fig. 4. Upper panel: simulated zonal mean TEC (background contour plot) and input F10.7 index (line plot) for (a) low and (b) high solar activity conditions. Lower panel: corresponding cross-correlation plots between the F10.7 index and modeled GTEC.

4. Summary and Conclusion

We analyzed GTEC and solar proxies datasets to investigate the ionospheric behavior during low (2007-2009) and high (2013-2015) solar activity years. The correlation between GTEC and SEE integrated EUV flux was stronger during high solar activity years than during low solar activity years. Whereas, the F10.7 index results in weaker correlation. An ionospheric delay of about 1 day in GTEC against solar parameters during both low and high solar activity years is observed. As shown by cross-wavelet analysis, EUV flux and F10.7 index show similar characteristics of correlation with GTEC during low and high solar activity years. From this analysis, it is clearly visible that solar radiation is strongly influencing the GTEC at the 27 days solar rotation period.

We have used the CTIPe model to simulate GTEC during low and high solar activity conditions. The experiment was performed using the F10.7 index for low (70-75 sfu) and high (100-140 sfu) solar activity for 15 March 2013 conditions. Preliminary results using cross-correlation analysis show an ionospheric delay of 1 day in GTEC with respect to the F10.7 index during both low and high solar activity. In comparison to low solar activity, a weaker correlation has been observed during high solar activity. In this first approach, we have found that the CTIPe model is able to reproduce the

observed ionospheric delay. In further studies, we will also analyze photodissociation and ionization processes of atomic oxygen, molecular oxygen, and molecular nitrogen to check the validity of the results by Jakowski et al. (1991).

Acknowledgements

IGS TEC maps have been kindly provided via NASA through ftp://cddis.gsfc.nasa.gov/gnss/products/ionex/. Daily F10.7 indices and TIMED/SEE version 3A spectra have been provided by LASP at http://lasp.colorado.edu/lisird/noaa_radio_flux and http://lasp.colorado.edu/lisird/data/timed_see_ssi_l3a, respectively. Mg-II indices have been provided by IUP at www.iup.uni-bremen.de/UVSAT/Datasets/mgii. The study has been supported by Deutsche Forschungsgemeinschaft (DFG) through grant No. JA 836/33-1.

References

Afraimovich, E. L., Astafyeva, E. I., Oinats, A. V., Yasukevich, Yu. V., Zhivetiev, I. V., 2008: Global electron content: a new conception to track solar activity, Ann. Geophys., 26, 335–344, doi:10.5194/angeo-26-335-2008.

Akmaev, R. A., 2011: Whole atmosphere modeling: Connecting terrestrial and space weather, Rev. Geophys., 49, RG4004, doi:10.1029/2011RG000364.

Appleton, E. V., 1946: Two anomalies in the ionosphere, Nature, 157, 691. doi:10.1038/157691a0.

Astafyeva, E.I., Afraimovich, E.L., Oinats, A.V., Yasukevich, Y.V., Zhivetiev, I.V., 2008: Dynamics of global electron content in 1998–2005 derived from global GPS data and IRI modeling, Adv. Space Res., 42(4), 763-769.

BenMoussa, A., S. Gissot, U. Schühle, G. Del Zanna, F. Auchère, et al., 2013: On-orbit degradation of solar instruments, Sol. Phys., 288, 389–434, DOI: 10.1007/s11207-013-0290-z.

CDDIS: GNSS Atmospheric Products, available at: http://cddis.nasa.gov/Data_and_Derived_Products/GNSS/atmospheric_products.html, last access: 29 January, 2017.

Chen, Y., Liu, L., Le, H., Zhang, H., 2015: Discrepant responses of the global electron content to the solar cycle and solar rotation variations of EUV irradiance, Earth, Planets and Space, 67(1), 80.

Chen, Y., Liu, L., Wan, W., 2011: Does the F10.7 index correctly describe solar EUV flux during the deep solar minimum of 2007–2009? J. Geophys. Res., 116, A04304, doi:10.1029/2010JA016301.

Codrescu, M. V., Fuller-Rowell, T. J., Munteanu, V. , Minter, C. F., Millward G. H., 2008: Validation of the coupled thermosphere ionosphere plasmasphere electrodynamics model: CTIPe-Mass Spectrometer Incoherent Scatter temperature comparison, Space Weather, 6, S09005, doi:10.1029/2007SW000364.

Codrescu, M. V., Negrea, C., Fedrizzi, M., Fuller-Rowell, T. J., Dobin, A., Jakowsky, N., Khalsa,H., Matsuo, T., Maruyama, N., 2012: A real-time run of the Coupled Thermosphere Ionosphere Plasmasphere Electrodynamics (CTIPe) model, Space Weather, 10, S02001, doi:10.1029/2011SW000736.

DeWolfe, A. W., Wilson, A., Lindholm, D. M., Pankratz, C. K., Snow, M. A., Woods,T. N., 2010: Solar Irradiance Data Products at the LASP Interactive Solar

Irradiance Datacenter (LISIRD), In AGU Fall255 Meeting 2010, Abstract GC21B-0881.

Dudok de Wit, T., Kretzschmar, M., Lilensten, J., Woods, T., 2009: Finding the best proxies for the solar UV irradiance, Geophys. Res. Lett., 36, L10107, doi:10.1029/2009GL037825.

Forbes, J. M., Palo, S. E., Zhang, X., 2000: Variability of the ionosphere, J. Atmos. Sol-Terr. Phy., 62(8), 685-693.

Fuller-Rowell, T. J. Rees, D., 1980: A three-dimensional time-dependent global model of the thermosphere. J. Atmos. Sci., 37, 2545–2567, doi:10.1175/1520-0469(1980)037<2545:ATDTDG>2.0.CO;2.

Fuller-Rowell, T. J., Rees, D., 1983: Derivation of a conservation equation for mean molecular weight for a two-constituent gas within a three-dimensional, time-dependent model of the thermosphere, Planet. Space 270 sci., 31(10), 1209-1222, doi: 10.1016/0032-0633(83)90112-5.

Grinsted, A., Moore, J. C., Jevrejeva, S., 2004: Application of the cross wavelet transform and wavelet coherence to geophysical time series, Nonlinear proc. Geoph., 11(5/6), 561-566.

Guo J, Li W, Liu X, Kong Q, Zhao C, Guo B., 2015: Temporal-Spatial Variation of Global GPS- Derived Total Electron Content, 1999–2013. PLoS ONE 10(7): e0133378. doi:10.1371/journal.pone.0133378.

Hernandez-Pajares, M., Juan, J. M., Sanz, J., Orus, R., Garcia-Rigo, A., Feltens, J., Komjathy, A., Schaer, S. C., Krankowski, A., 2009: The IGS VTEC maps: a reliable source of ionospheric information since 1998, J. Geod., 83, 263–275.

Jacobi, C., Jakowski, N., Schmidtke, G., Woods, T. N., 2016: Delayed response of the global total electron content to solar EUV variations, Advances in Radio Science: ARS, 14, 175.

Jakowski, N., Fichtelmann, B., Jungstand, A., 1991: Solar activity control of Ionospheric and thermospheric processes, J. Atmos. Terr. Phys., 53, 1125–1130.

Kane, R. P., 1992: Sunspots, solar radio noise, solar EUV and ionospheric foF2, J. Atmos. Terr. Phy., 54(3-4), 463-466.

Lee, C. K., Han, S. C., Bilitza, D., Seo, K. W., 2012: Global characteristics of the correlation and time lag between solar and ionospheric parameters in the 27-day period, J. Atmos. Sol-Terr. Phys., 77, 219-224.

Liu, J. Y., Chen, Y. I., Lin, J. S., 2003: Statistical investigation of the saturation effect in the ionospheric foF2 versus sunspot, solar radio noise, and solar EUV radiation, J. Geophys. Res., 108(A2), 1067, doi:10.1029/2001JA007543.

Liu, L., Chen, Y., 2009: Statistical analysis of solar activity variations of total electron content derived at Jet Propulsion Laboratory from GPS observations, J. Geophys. Res., 114, A10311, doi:10.1029/2009JA014533.

Liu, L., Wan, W., Ning, B., Pirog, O. M., and Kurkin V. I., 2006: Solar activity variations of the ionospheric peak electron density, J. Geophys. Res., 111, A08304, doi:10.1029/2006JA011598.

Maruyama, T., 2010: Solar proxies pertaining to empirical ionospheric total electron content models, J. Geophy. Res., 15, A04306, doi:10.1029/2009JA014890.

Millward, G. H., Moffett, R. J., Quegan, S., Fuller-Rowell, T. J., 1996: A coupled thermosphere-ionosphere-plasmasphere model (CTIP), in Solar-Terrestrial Energy Pro-

gram: Handbook of Ionospheric Models, edited by R. W. Schunk. PP. 239–279, Cent. for Atmos. and Space Sci., Utah State Univ., Logan, Utah.

Min, K., Park, J., Kim, H., Kim, V., Kil, H., Lee, J., Rentz, S., Lühr, H., Paxton, L., 2009: The 27-day modulation of the low-latitude ionosphere during a solar maximum, J. Geophys. Res., 114, A04317, doi:10.1029/2008JA013881.

Mukhtarov, P., Pancheva, D., Andonov, B., Pashova, L., 2013: Global TEC maps based on GNSS data: 1. Empirical background TEC model, J. Geophys. Res., 118, doi:10.1002/jgra.50413.

Patel, N. C., Karia, S. P., Pathak, K.N., 2017: GPS-TEC variation during low to high solar activity period (2010-2014) under the northern crest of Indian equatorial ionization anomaly region, Positioning, 8, 13-35. doi10.4236/pos.2017.82002.

Quegan, S., Bailey, G. J., Moffett, R. J., Heelis, R. A., Fuller-Rowell, T. J., Rees, D., Spiro, R. W., 1982: A theoretical study of the distribution of ionization in the high-latitude ionosphere and the plasmasphere: First results on the mid-latitude trough and the light-ion trough, J. Atmos. Terr. Phys., 44(7), 619–640, doi:10.1016/0021-9169(82)90073-3.

Richards, P. C., Fennelly, J. A., Torr, D. G. 1994: EUVAC: A solar EUV flux model for aeronomic calculations, J. Geophys. Res., 99, 8981–8992, doi:10.1029/94JA00518.

Richmond, A. D., Ridley, E. C., Roble, R. G., 1992: A thermosphere/ionosphere general circulation model with coupled electrodynamics, Geophys. Res. Lett., 19(6), 601–604, doi:10.1029/92GL00401.

Ridley, A.J., Deng, Y., Toth, G., 2006: The global ionosphere–thermosphere model, J. Atmos. Sol. Terr. Phy., 68(8), 839-864.

Snow, M., Weber, M., Machol, J., Viereck, R., Richard, E., 2014: Comparison of Magnesium II core-to-wing ratio observations during solar minimum 23/24, J. Space Weather Space Clim., 4, A04, doi:10.1051/swsc/2014001.

Su, Y. Z., Bailey, G. J., Fukao, S., 1999: Altitude dependencies in the solar activity variations of the ionospheric electron density, J. Geophy. Res., 104(A7), 14879-14891.

Tapping, K. F., 2013: The 10.7 cm solar radio flux (F10.7), Space Weather, 11, 394–406, doi:10.1002/swe.20064.

Wolf, R., 1856: Mittheilungen über die Sonnenflecken, Vierteljahresschrift der Naturforschenden Gesellschaft in Zürich, 1, 151-161.

Woods, T. N., Bailey, S., Eparvier, F., Lawrence, G., Lean, J., McClintock, B., Roble, R., Rottmann, G. J., Solomon, S. C., Tobiska, W. K., White, O. R., 2000: TIMED Solar EUV Experiment, Phys. Chem. Earth, Part C, 25, 393–396, doi:10.1016/S1464-1917(00)00040-4.

Woods, T. N., Eparvier, F., Bailey, S., Chamberlin, P., Lean, J., Rottmann, G. J., Solomon, S. C., Tobiska, W. K., Woodraska, D. L., 2005: Solar EUV Experiment (SEE): Mission overview and first results, J. Geophys. Res., 110, A01312, doi:10.1029/2004JA010765.